Journal of
Ceramic Science
and Technology

J. Ceram. Sci. Tech., 07 [04] 341-348 (2016)
DOI: 10.4416/JCST2016-00040
available online at: http://www.ceramic-science.com

Effects of Micro-Damage on the Nonlinear Constitutive Behavior of SiC/SiC Minicomposites

S. Zhang[1, 2], X. Gao[*1, 2], J. Chen[1, 2], H. Dong[1, 2], Y. Song[1, 2, 3], H. Zhang[4]

[1]Jiangsu Province Key Laboratory of Aerospace Power System, College of Energy and Power Engineering, Nanjing University of Aeronautics and Astronautics, Nanjing 210016, P.R. China
[2]Key Laboratory of Aero-engine Thermal Environment and Structure, Ministry of Industry and Information Technology, Nanjing 210016, P.R. China
[3]State Key Laboratory of Mechanics and Control Mechanical Structures, Nanjing University of Aeronautics and Astronautics, Nanjing 210016, P.R. China
[4]Military Representative Office Stationed 420 Factory, Chengdu 610503, P.R. China
received May 27, 2016; received in revised form July 14, 2016; accepted July 19, 2016

Abstract

The effects of matrix cracking, fiber/matrix interfacial debonding and fiber fracture on the nonlinear constitutive behavior of SiC/SiC minicomposites were studied. An *in-situ* tensile test was performed to detect the matrix cracking in real time. The macroscopic tensile test was also performed on the SiC/SiC minicomposites to obtain their stress-strain responses. Based on the test results, models of these types of damage were developed. The shear-lag model was adopted to simulate the stress-strain response of SiC/SiC minicomposites. The contributions of these types of damage to the nonlinearity were discussed. The experimental and numerical results showed that fiber fracture occurs near the ultimate stress of minicomposites and that the nonlinear behavior of SiC/SiC minicomposites is primarily caused by matrix cracking and interfacial debonding. In addition, the mechanical behavior will recover its linearity after the saturation of matrix cracks and the complete debonding of the interface.

Keywords: Ceramic matrix composites, nonlinearity, micro-damage, matrix cracks, in-situ mechanical testing

I. Introduction

Owing to their excellent mechanical behavior at elevated temperatures, SiC/SiC composites are the materials with the highest potential for use in high-temperature parts of aeronautical vehicles [1]. The SiC/SiC minicomposite is defined as the combination of a SiC fiber bundle, the SiC matrix that surrounds the fibers and the interface between the SiC fiber and the matrix [2]. The minicomposite is the most important component of the SiC/SiC composite because it bears most of the external load [3–7]. Moreover, since the composite can be seen as reinforced by the minicomposite, its mechanical behavior is influenced by that of the minicomposite. Thus, in recent years, the mechanical behaviors of minicomposites have received substantial attention.

Sauder [8], Jacques [9], Morscher [10] and Bertrand [11] performed tensile tests on minicomposites and found that they had a nonlinear constitutive behavior. In addition, they found that there is a second linear region after the nonlinear region on the stress-strain curve. For a better understanding of the nonlinear constitutive behavior, some researchers have studied the microscopic damage of minicomposites upon loading.

Chateau *et al.* [12] observed matrix cracking at various strain states using an *in-situ* scanning electron microscopic (SEM) tensile test. They also observed a few fiber failures using an *in-situ* X-ray microtomography tensile test [13]. Maillet *et al.* [14] proposed a testing protocol that combines acousto-ultrasonics (AU) and acoustic emission (AE) monitoring and provided a global measure of matrix cracking damage. Jacques *et al.* [9] found debonding in the fiber/matrix interface based on SEM observation of the failure surfaces of minicomposites.

In these works, it was observed that matrix cracking, fiber/matrix interfacial debonding and fiber fracture were the primary damage patterns for minicomposites. However, effects of these forms of damage on the nonlinearity of minicomposites were not studied due to a lack of damage models.

Other researchers focused on the effects of constituents on the mechanical behavior of minicomposites. Sauder *et al.* [8] studied the influence of interface characteristics on the mechanical properties of minicomposites. Morscher *et al.* [10] studied the mechanical behaviors of minicomposites reinforced by several types of SiC fibers. They found that fibers affect the ultimate strength, the strain to failure and the interfacial shear strength of minicomposites.

However, constituent properties have no direct connection to the damage patterns and therefore these works have not revealed the amount that these damage patterns contribute to nonlinearity. This is important to better under-

* Corresponding author: gaoxiguang@nuaa.edu.cn

stand and model the damage of minicomposites. Moreover, the cause of the second linear region has not been demonstrated theoretically.

In the present study, the effects of matrix cracking, interfacial debonding and fiber fracture on the nonlinearity of SiC/SiC minicomposites were studied. An *in-situ* tensile test was performed to detect the matrix cracking in real time. The macroscopic tensile test was also performed on the minicomposites to obtain their stress-strain responses. Based on the test results, the models of these types of damage were developed, and the contributions of these types of damage to the nonlinearity were discussed. A comparison of the stress-strain responses of different fiber fracture processes showed that the fiber fracture occurred almost simultaneously in the present study, which was not the same as the phenomenon observed in the mentioned studies. Both the experimental results and the theoretical calculation indicated that fiber fracture does not contribute to the nonlinear behavior of the present minicomposites and that the nonlinear behavior is mainly caused by matrix cracking and interfacial debonding. In addition, it was demonstrated that the mechanical behavior will recover its linearity (the second linear region on the stress-strain curve) after the saturation of matrix cracks and the complete debonding of the interface.

II. Materials and Experimental Procedure

(1) Materials

The SiC/SiC minicomposites were provided by the Institute of Metal Research, Chinese Academy of Sciences. The samples were manufactured using the chemical vapor infiltration (CVI) process, which deposited the pyrocarbon interphase and SiC matrix onto the SiC fiber bundle. The material property data of the samples are listed in Table 1. In Table 1, the subscripts f and m denote the fiber and matrix, respectively. In addition, E is the elasticity modulus, v is the volume fraction, a is the coefficient of thermal expansion, r is the diameter of SiC fiber and ΔT is the variation between room temperature and the operation temperature. Note that in Table 1, the volume fraction v_f and v_m were determined from the mass of each constituent. E_f was obtained with the tensile test on the SiC fiber bundle, E_m was obtained with the nanoindentation experiment and r_f was measured by means of SEM. The standard deviations of these parameters are also provided to reflect the scatter. a_f, a_m and ΔT were quoted from the literature [8, 15].

(2) Tensile test

A unidirectional tensile test on the SiC/SiC minicomposites (Fig. 1) was performed at room temperature under a constant displacement rate of 0.05 mm/min. The load was measured by a 300-N load cell, and the deformation was measured with an extensometer with a 25-mm gauge length.

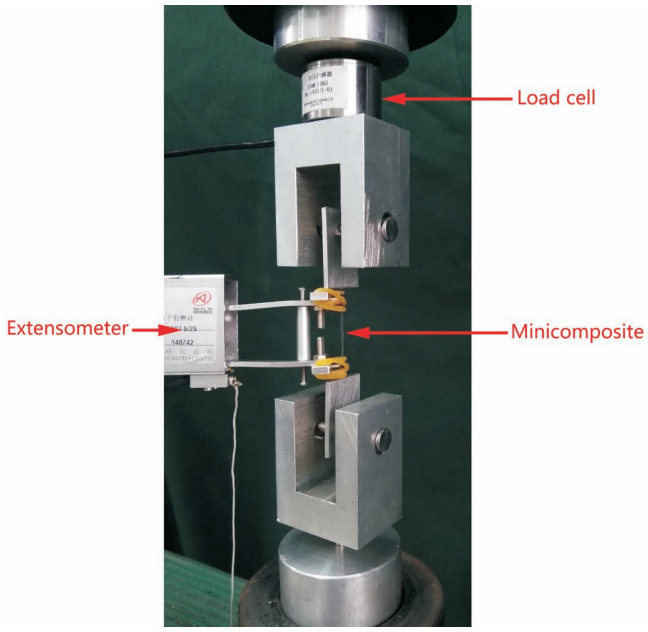

Fig. 1: Tensile test of the SiC/SiC minicomposites.

(3) Real-time matrix crack detection

Real-time matrix crack detection was conducted using the *in-situ* tensile test. The minicomposite sample (with a 25-mm gauge length) was clamped in a specific loading apparatus that could hold the sample and measure the load. The loading equipment was placed below the lens of a digital microscope (Fig. 2). The tensile process was interrupted at various loads to observe and record the number of matrix cracks until the ultimate failure. At each step, the load was measured using the load cell and the matrix cracks were observed through the digital microscope. The present study was focused on the gauge length, which allowed the observation of a significant number of matrix cracks. After the number of the matrix cracks was counted, the tensile process was continued. On the basis of the division of the number by the gauge length, the matrix crack densities under different stress levels can be obtained.

Table 1: Material properties of SiC/SiC minicomposites.

Item	Mean value	Standard deviation	Item	Mean value	Standard deviation
E_f/GPa	160	7.0	E_m/GPa	190	22.7
v_f	0.23	0.03	v_m	0.77	0.03
a_f/×10^{-6}/°C	3.1	-	a_m/×10^{-6}/°C	4.6	-
r_f/μm	6.5	0.12	ΔT/°C	-1000	-

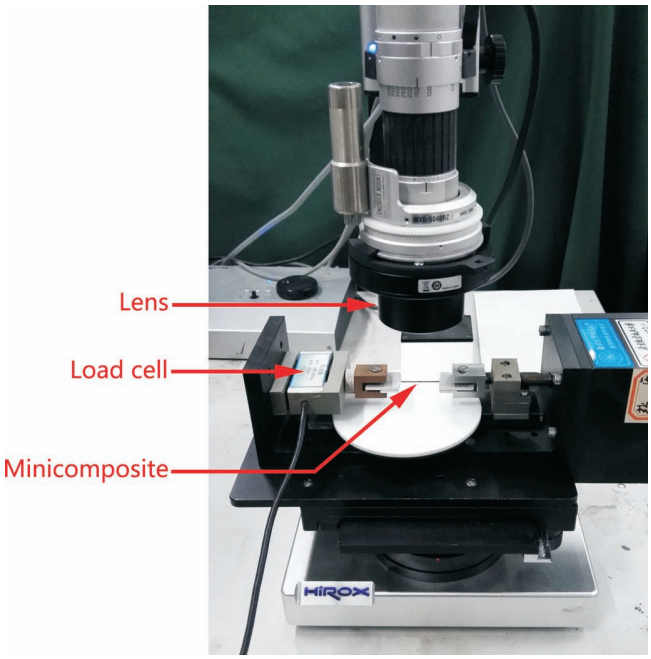

Fig. 2: Real-time matrix crack detection.

III. Modeling of the Micro-Damage

(1) Interfacial debonding

Owing to its low fracture toughness, the ceramic matrix first cracks under the tensile load. In the plane of the matrix cracks, the fiber carries the entire load, which causes fiber/matrix interfacial debonding to occur near the plane of the matrix cracks. In the debonded region, the interfacial shear stress τ is constant and transfers the normal stress back into the matrix. According to the shear-lag model [16, 17, 18], the distribution of the fiber's normal stress in the debonded ($L/2\text{-}d \le |x| \le L/2$) and bonded ($|x| \le L/2\text{-}d$) regions is shown in Fig. 3 and described by Eq. (1).

$$\sigma_f(x) = \begin{cases} \dfrac{\sigma}{v_f} + \dfrac{2\tau}{r_f}\left(x - \dfrac{L}{2}\right), & L/2 - d \le |x| \le L/2 \\ \sigma_{f0}, & |x| \le L/2 - d \end{cases} \quad (1)$$

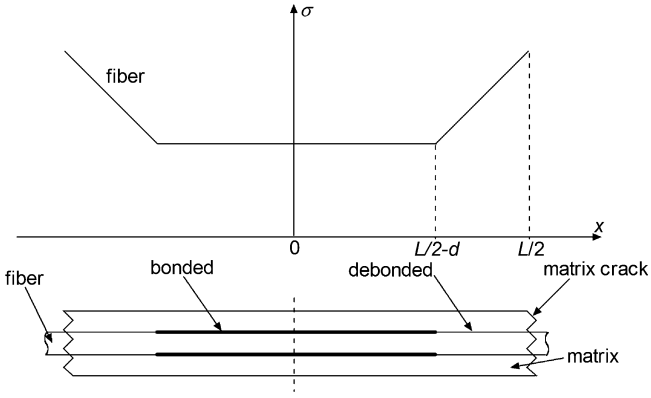

Fig. 3: Stress distributions in the debonded and bonded regions.

In this equation, L is the matrix crack spacing, σ_{f0} is the normal stress if the composite is undamaged and d is the length of the debonded region.

$$\sigma_{f0} = \frac{E_f}{E_c}\sigma + E_f(\alpha_c - \alpha_f)\Delta T \quad (2)$$

$$d = \frac{r_f}{2\tau}\left(\frac{\sigma}{v_f} - \sigma_{f0}\right) \quad (3)$$

where E_c is the composite elasticity modulus and a_c is the composite coefficient of thermal expansion.

$$E_c = v_f E_f + v_m E_m \quad (4)$$

$$\alpha_c = \frac{\alpha_f v_f E_f + \alpha_m v_m E_m}{E_c} \quad (5)$$

As shown in Eq. (3), the length of the debonded region increases with the increase in the applied stress until the interface is debonded completely, i.e. $d = L/2$. When the interface is debonded completely, the stress distribution is expressed as follows:

$$\sigma_f(x) = \frac{\sigma}{v_f} + \frac{2\tau}{r_f}\left(x - \frac{L}{2}\right), \quad |x| \le L/2 \quad (6)$$

(2) Fiber fracture

Fig. 4 shows the stress-strain curve of SiC/SiC minicomposites obtained with the above tensile test. The curve can be divided into three regions: the initial linear elastic region, the nonlinear region and the second linear region. The stress range of the nonlinear region is approximately 75 ~ 200 MPa. In contrast to the results of previous studies [19, 20], a second nonlinear region was not observed before the fracture. This result shows that the gradual fiber fracture is not obvious for the minicomposites in the present study. A detailed analysis regarding the effects of the fiber fracture is presented in the Section ***Effects of fiber fracture***.

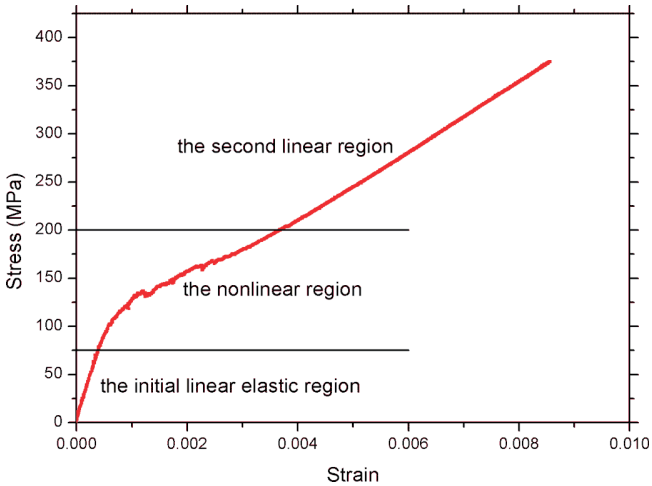

Fig. 4: The stress-strain curve of the SiC/SiC minicomposites.

The fiber fracture process is well described by the Weibull distribution [21]. For a two-parameter Weibull distribution, the percentage of fractured fibers P is as follows:

$$P = 1 - \exp\left[-\left(\frac{\sigma}{\sigma_0^f}\right)^{m_f}\right] \quad (7)$$

where σ_0^f and m_f are the statistical parameters. Once a fiber is fractured, it is no longer capable of carrying the load. Therefore, the volume fraction of fibers can be regarded as $(1\text{-}P)v_f$.

(3) Matrix cracking

The matrix crack densities (number of matrix cracks per unit length) under different loading levels can be obtained by means of the above real-time matrix crack detection. Fig. 5 shows a representative image of matrix cracks observed with a digital microscope.

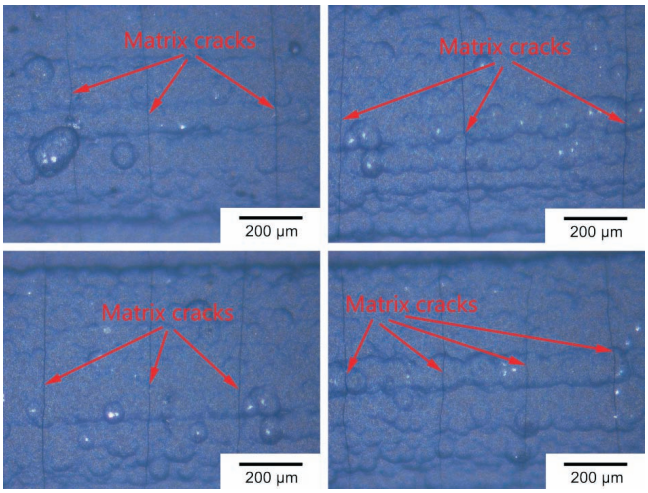

Fig. 5: A representative image of the matrix cracks.

The matrix crack densities under different stress levels are presented in Fig. 6. The evolution rate of the matrix cracks initially increases and then decreases as the saturation of the cracks (i.e., when the crack density remains unchanged) is reached rapidly. The stress range for the matrix cracks to propagate rapidly in Fig. 6 is 75 ~ 200 MPa. Note that this range is also the range of the nonlinear region of the stress-strain curve (Fig. 4). This result shows that the nonlinearity of the unidirectional tensile behavior is related to the evolution of matrix cracks.

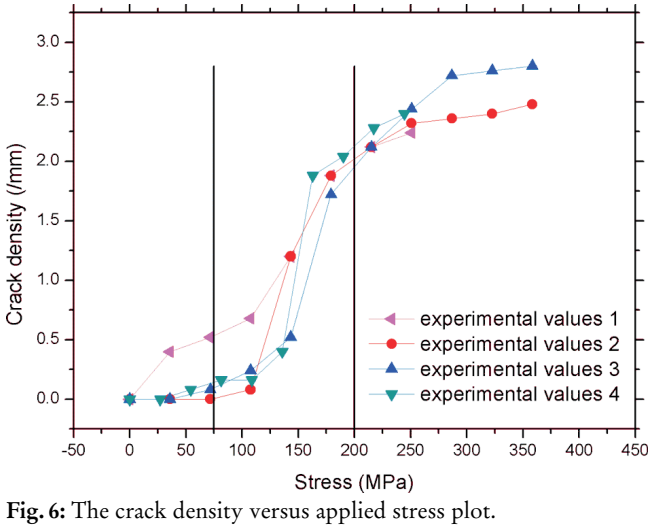

Fig. 6: The crack density versus applied stress plot.

There are some failure criteria in the literature [16, 22–24] for modeling the matrix cracking process. In the present study, matrix cracking models are also based on the Weibull distribution. The matrix crack density at the applied stress σ can be expressed as follows:

$$D = D_{sat}\left\{1-\exp\left[-\left(\frac{\sigma}{\sigma_0^m}\right)^{m_m}\right]\right\} \tag{8}$$

where m_m and σ_0^f are the statistical parameters, and D_{sat} is the final density when crack saturation is reached. In the present study, $m_m = 5$, $= 160$ MPa and $D_{sat} = 2.5$ mm^{-1}. As shown in Fig. 7, the predicted crack density versus applied stress plot matches well with the empirical data.

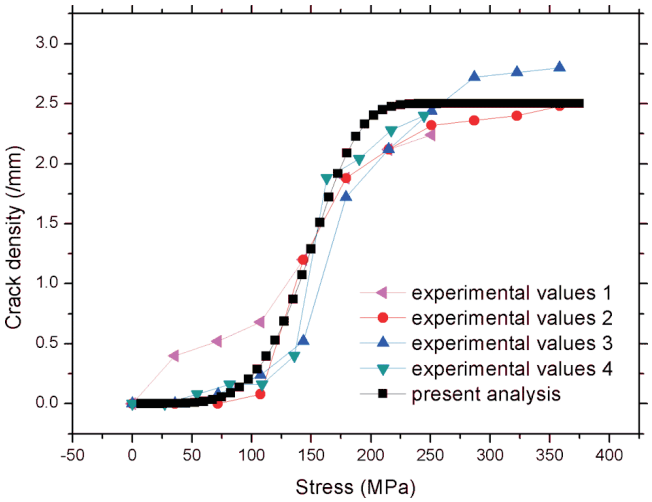

Fig. 7: The predicted crack density.

IV. Results and Discussion

(1) Stress-strain response

The minicomposites' average strain $\bar{\varepsilon}_c$ can be seen as equivalent to the average strain of the undamaged fibers $\bar{\varepsilon}_f$.

$$\begin{aligned}\bar{\varepsilon}_c &= \bar{\varepsilon}_f \\ &= \frac{2}{E_f L}\int_0^{L/2}\sigma_f(x)dx + (\alpha_f - \alpha_c)\Delta T \\ &= \frac{2}{E_f L}\left[\int_0^{L/2-d}\sigma_{f0}dx + \int_{L/2-d}^{L/2}\left(\frac{\sigma}{\nu_f} + \frac{2\pi}{r_f}\left(x - \frac{L}{2}\right)\right)dx\right] \\ &\quad + (\alpha_f - \alpha_c)\Delta T \\ &= \frac{2}{E_f L}\left[\frac{\sigma}{\nu_f}d - \frac{\pi}{r_f}d^2 + \sigma_{f0}\left(\frac{L}{2} - d\right)\right] + (\mathrm{alpha}_f - \alpha_c)\Delta T\end{aligned} \tag{9}$$

When the interface is completely debonded, the average strain is expressed as follows:

$$\begin{aligned}\bar{\varepsilon}_c &= \bar{\varepsilon}_f \\ &= \frac{2}{E_f L}\int_0^{L/2}\sigma_f(x)dx + (\alpha_f - \alpha_c)\Delta T \\ &= \frac{2}{E_f L}\int_0^{L/2}\left[\frac{\sigma}{\nu_f} + \frac{2\pi}{r_f}\left(x - \frac{L}{2}\right)\right]dx + (\alpha_f - \alpha_c)\Delta T \\ &= \frac{\sigma}{\nu_f E_f} - \frac{\pi L}{2 r_f E_f} + (\alpha_f - \alpha_c)\Delta T\end{aligned} \tag{10}$$

The stress-strain response can be calculated using Eqs. (9) and (10). The percentage of fractured fibers P and the matrix crack spacing L are determined with the models in Sections ***Fiber fracture*** and ***Matrix cracking***. As shown in Eq. (10), τ can be determined from the intercept of the second linear region. In the present study, τ = 15 MPa. For the fiber fracture model in the present study, σ_0^f and $m_f = 24$. A comparison between the stress-strain response determined with the present analysis and the experimental results under monotonic loading is presented in Fig. 8. The

present analysis and the experimental values are in good agreement.

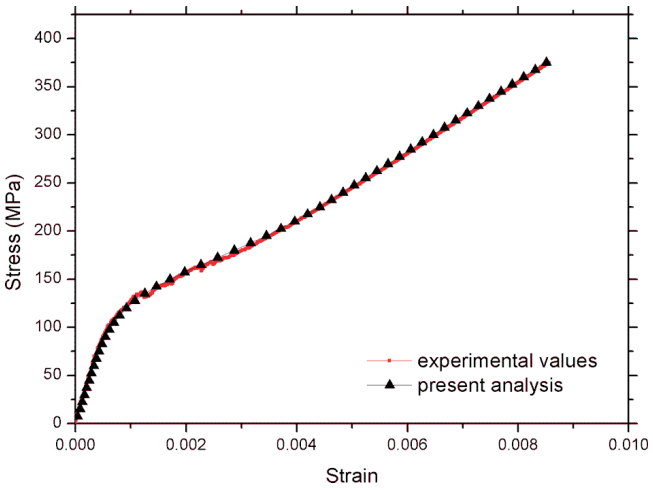

Fig. 8: The predicted stress-strain response and the experimental results.

The first turning point in the stress-strain curve occurs near $\sigma = 75$ MPa, followed by a decrease in stiffness, which is caused by the propagation of matrix cracks. The second turning point is near σ =200 MPa, and then, the stress-strain curve recovers its linearity due to the saturation of matrix cracks and the completely debonded interface.

(2) Effects of fiber fracture

To verify the effects of fiber fracture, the stress-strain responses of different σ_0^f values are presented. As shown in Fig. 9, the fiber fracture has no effect on the first nonlinear region and primarily affects the second nonlinear region. With a high σ_0^f, the second nonlinear region is not obvious because all the fibers fracture almost simultaneously. This result also indicates that the fiber fracture does not contribute to the nonlinearity of minicomposites in the present study.

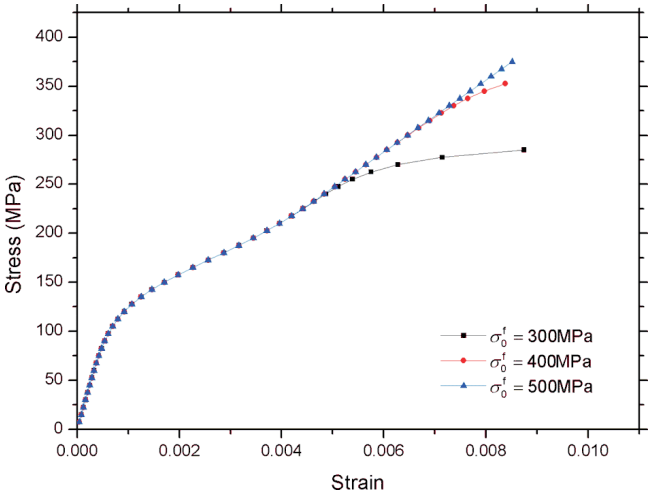

Fig. 9: The stress-strain responses of different fiber fracture processes.

(3) Effects of matrix cracking

The stress-strain responses of different saturated matrix crack densities are calculated. As shown in Fig. 10, the nonlinearity is not obvious with a low crack density. Without matrix cracking (D_{sat}=0), the minicomposites will remain linear until they reach the ultimate strength; thus, the matrix cracking substantially contributes to the nonlinear constitutive behavior of minicomposites. Note that for D_{sat} = 2.5 mm^{-1} and D_{sat} = 4 mm^{-1}, the slopes of the second linear regions are the same because the slope will recover to $v_f E_f$ after the interface is debonded completely, as shown in Eq. (10). For D_{sat} = 0.4 mm^{-1}, the interface will not be debonded completely before reaching the ultimate strength due to the relatively longer crack spacing. Therefore, Eq. (10) is not valid, and the slope of the stress-strain curve will not recover to $v_f E_f$.

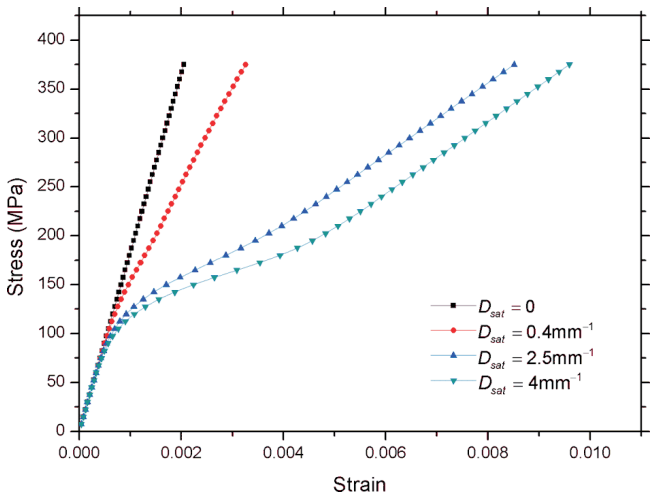

Fig. 10: The stress-strain responses of different saturated matrix crack densities.

(4) Effects of interfacial debonding

Eq. (3) indicates that the debonded length is inversely proportional to the interfacial shear stress. To verify the effects of interfacial debonding, the stress-strain responses of different interfacial shear stresses are presented in Fig. 11.

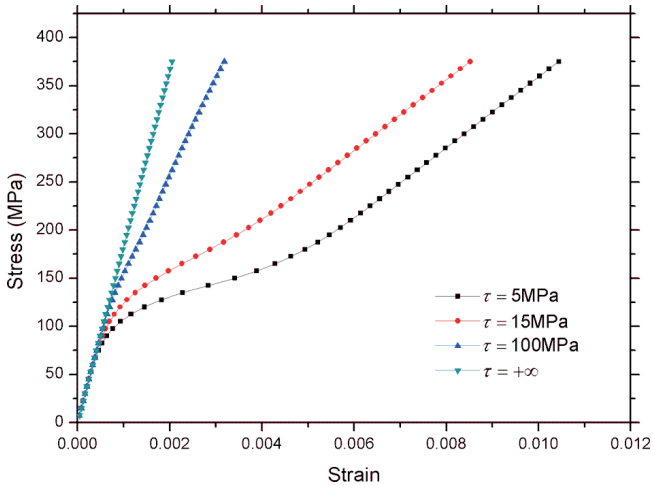

Fig. 11: The stress-strain responses of different interfacial shear stresses.

As shown in Fig. 11, the nonlinearity is not obvious with a high interfacial shear stress. When the interfacial shear stress tends to infinity, the debonded length is as follows:

$$d = \frac{r_f}{2\pi}\left(\frac{\sigma}{v_f} - \sigma_{f0}\right) = \frac{r_f}{2(\infty)}\left(\frac{\sigma}{v_f} - \sigma_{f0}\right) = 0 \qquad (11)$$

The minicomposite average strain determined with Eq. (9) is as follows:

$$\begin{aligned}\bar{\varepsilon}_c &= \frac{2}{E_f L}\left[\frac{\sigma}{v_f}d - \frac{\pi}{r_f}d^2 + \sigma_{f0}\left(\frac{L}{2} - d\right)\right] + (\alpha_f - \alpha_c)\Delta T \\ &= \frac{\sigma_{f0}}{E_f} + (\alpha_f - \alpha_c)\Delta T \\ &= \frac{1}{E_f}\left[\frac{E_f}{E_c}\sigma + E_f(\alpha_c - \alpha_f)\Delta T\right] + (\alpha_f - \alpha_c)\Delta T \\ &= \frac{\sigma}{E_c}\end{aligned} \tag{12}$$

Eq. (12) demonstrates that the constitutive behavior will always be linear when there is no interfacial debonding (i.e. the interfacial shear stress tends to infinity). Thus, the interfacial debonding substantially contributes to the nonlinear constitutive behavior of the minicomposites.

V. Conclusions

When under loading, SiC/SiC minicomposites exhibit a nonlinear behavior along with matrix cracking, fiber/matrix interfacial debonding and fiber fracture. To study the effects of these forms of micro-damage on nonlinearity, a macroscopic tensile test was performed on the SiC/SiC minicomposites. Real-time matrix crack detection was also conducted using an *in-situ* tensile test. Based on the test results, the characteristics, models and effects of these micro-damages were discussed.

The following conclusions were drawn regarding the effects of these forms of micro-damage on the nonlinearity of SiC/SiC minicomposites:

1) Fiber fracture has no effect on the first nonlinear region of the stress-strain curves and primarily affects the second nonlinear region. A comparison of the stress-strain responses of different fiber fracture processes showed that all the fibers fractured almost simultaneously in the present study. Thus, fiber fracture does not contribute to the nonlinearity of the present minicomposites.
2) Without matrix cracking, the minicomposites will remain linear until they reach the ultimate strength. This behavior indicates that the matrix cracking process contributes to the nonlinear constitutive behavior of minicomposites.
3) The interfacial debonding also contributes to the nonlinearity because the constitutive behavior is always linear when there is no interfacial debonding.
4) The mechanical behavior will recover its linearity after the saturation of matrix cracks and the complete debonding of the interface.

Acknowledgements

This work was supported by the National Natural Science Foundation of China [51575261], the Aeronautical Science Foundation of China [2015ZB52015], the NUAA Fundamental Research Funds [NS2013022], the Fundamental Research Funds for the Central Universities [NZ2014402], the Funding of Jiangsu Innovation Program for Graduate Education [KYLX_0300], the Fundamental Research Funds for the Central Universities and the Priority Academic Program Development of Jiangsu Higher Education Institutions.

References

1 Naslain, R.: Design, preparation and properties of non-oxide CMCs for application in engines and nuclear reactors: an overview, *Compos. Sci. Technol.*, **64**, 155 – 170, (2004).

2 Naslain, R., Lamon, J., Pailler, R., Bourrat, X., Guette, A., Langlais, F.: Micro/minicomposites: a useful approach to the design and development of non-oxide CMCs, *Compos. Part A.*, **30**, 537 – 547, (1999).

3 Gélébart, L., Chateau, C., Bornert, M., Crépin, J., Boller, E.: X-ray tomographic characterization of the macroscopic porosity of chemical vapor infiltration SIC/SIC Composites: effects on the elastic behavior, *Int. J. Appl. Ceram. Tec.*, **7**, 348 – 360, (2010).

4 Xu, Y.J., Zhang, W.H., Domaszewski, M.: Microstructure modelling and prediction of effective elastic properties of 3D multiphase and multilayer braided composite, *Mater. Sci. Techlond.*, **27**, 1213 – 1221, (2011).

5 Yanjun, C., Guiqiong, J., Bo, W., Wei, L.: Elastic behavior analysis of 3D angle-interlock woven ceramic composites, *Acta. Mech. Solida. Sin.*, **19**, 152 – 159, (2006).

6 Tang, C., Blacklock, M., Hayhurst, D.R.: Stress-strain response and thermal conductivity degradation of ceramic matrix composite fiber tows in 0 – 90° uni-directional and woven composites, *J. Compos. Mater.*, **45**, 1461 – 1482, (2011).

7 Morscher, G.N.: Modeling the elastic modulus of 2D woven CVI SiC composites, *Compos. Sci. Technol.*, **66**, 2804 – 2814, (2006).

8 Sauder, C., Brusson, A., Lamon, J.: Influence of interface characteristics on the mechanical properties of hi-nicalon type-S or Tyranno-SA3 fiber-reinforced SiC/SiC minicomposites, *Int. J. Appl. Ceram. Tec.*, **7**, 291 – 303, (2010).

9 Jacques, S., Lopez-Marure, A., Vincent, C., Vincent, H., Bouix, J.: SiC/SiC minicomposites with structure-graded BN interphases, *J. Eur. Ceram. Soc.*, **20**, 1929 – 1938, (2000).

10 Morscher, G.N., Martinez-Fernandez, J.: Fiber effects on minicomposite mechanical properties for several silicon carbide fiber-chemically vapor-infiltrated silicon carbide matrix systems, *J. Am. Ceram. Soc.*, **82**, 145 – 155, (1999).

11 Bertrand, S., Forio, P., Pailler, R., Lamon, J.: Hi-Nicalon/SiC minicomposites with (Pyrocarbon/SiC)n nanoscale multilayered interphases, *J. Am. Ceram. Soc.*, **82**, 2465 – 2473, (1999).

12 Chateau, C., Gélébart, L., Bornert, M., Crepin, J., Caldemaison, D., Boller, E., *et al.*: Experimental characterisation of damage in SiC/SiC minicomposites, *EPJ Web of Conferences*., **6**, 20002, (2010).

13 Chateau, C., Gélébart, L., Bornert, M., Crépin, J., Boller, E., Sauder, C., et al.: In situ X-ray microtomography characterization of damage in SiCf/SiC minicomposites, *Compos. Sci. Technol*., **71**, 916 – 924, (2011).

14 Maillet, E., Godin, N., R'Mili, M., Reynaud, P., Fantozzi, G., Lamon, J.: Damage monitoring and identification in SiC/SiC minicomposites using combined acousto-ultrasonics and acoustic emission, *Compos. Part A*., **57**, 8 – 15, (2014).

15 Solti, J.P., Robertson, D.D., Mall, S.: Estimation of interfacial properties from hysteretic energy loss in unidirectional ceramic matrix composites, *Adv. Compos. Mater.*, **9**, 161 – 173, (2000).

16 Lissart, N., Lamon,J.: Damage and failure in ceramic matrix minicomposites: experimental study and model, *Acta. Mater.*, **45**, 1025 – 1044, (1997).

17 Curtin, W.A., Ahn, B.K., Takeda, N.: Modeling brittle and tough stress-strain behavior in unidirectional ceramic matrix composites, *Acta. Mater.*, **46**, 3409 – 3420, (1998).

18 Chongdu, C., Holmes, J.W., Barber, J.R.: Estimation of interfacial shear in ceramic composites from frictional heating measurements, *J. Am. Ceram. Soc.*, **74**, 2802 – 2808, (1991).

[19] Chateau, C., Gélébart, L., Bornert, M., Crépin, J., Caldemaison, D., Sauder, C.: Modeling of damage in unidirectional ceramic matrix composites and multi-scale experimental validation on third generation SiC/SiC minicomposites, *J. Mech. Phys. Solids.*, **63**, 298 – 319, (2014).

[20] Curtin, W.A., Ahn, B.K., Takeda, N.: Modeling brittle and tough stress-strain behavior in unidirectional ceramic matrix composites, *Acta. Mater.*, **46**, 3409 – 3420, (1998).

[21] Weibull, W.: A statistical distribution function of wide applicability, *J. Appl. Mech-T ASME.*, **18**, 293 – 297, (1951).

[22] Carpinteri, A., Spagnoli, A., Vantadori, S.: A fracture mechanics model for a composite beam with multiple reinforcements under cyclic bending, *Int. J. Solids. Struct.*, **41**, 5499 – 5515, (2004).

[23] Gao, X., Zhang, S., Fang, G., Song, Y.: Distribution of slip regions on the fiber-matrix interface of ceramic matrix composites under arbitrary loading, *J. Reinf. Plast. Comp.*, **34**, 1713 – 1723, (2015).

[24] Curtin, W.A.: Multiple matrix cracking in brittle matrix composites, *Acta. Metal. Mater.*, **41**, 1369 – 1377, (1993).